processes

MDPI

Article

Transient Modeling and Performance Analysis of Hydrogen-Fueled Aero Engines

Xiting Wang, Ai He * and Zhongzhi Hu

Institute for Aero Engine, Tsinghua University, Beijing 100084, China
* Correspondence: heai@tsinghua.edu.cn; Tel.: +86-186-1041-8965

Abstract: With the combustor burning hydrogen, as well as the strongly coupled fuel and cooling system, the configuration of a hydrogen-fueled aero engine is more complex than that of a conventional aero engine. The performance, and especially the dynamic behavior of a hydrogen-fueled aero engine, need to be fully understood for engine system design and optimization. In this paper, both the transient modeling and performance analysis of hydrogen-fueled engines are presented. Firstly, the models specific to the hydrogen-fueled engine components and systems, including the hydrogen-fueled combustor, the steam injection system, a simplified model for a quick NOx emission assessment, and the heat exchangers, are developed and then integrated to a conventional engine models. The simulations with both Simulink and Speedgoat-based hardware in the loop system are carried out. Secondly, the performance analysis is performed for a typical turbofan engine configuration, CF6, and for the two hydrogen-fueled engine configurations, ENABLEH2 and HySIITE, which are currently under research and development by the European Union and Pratt & Whitney, respectively. At last, the simulation results demonstrate that the developed transient models can effectively reflect the characteristics of hydrogen burning, heat exchanging, and NOx emission for hydrogen-fueled engines. In most cases, the hydrogen-fueled engines show lower specific fuel consumption, lower turbine entry temperature, and less NOx emissions compared with conventional engines. For example, at max thrust state, the advanced hydrogen-fueled engine can reduce the parameters mentioned above by about 68.5%, 3.7%, and 12.7%, respectively (a mean value of two configurations).

Keywords: hydrogen-fueled aero engine; transient modeling; performance analysis

Citation: Wang, X.; He, A.; Hu, Z. Transient Modeling and Performance Analysis of Hydrogen-Fueled Aero Engines. *Processes* **2023**, *11*, 423. https://doi.org/10.3390/pr11020423

Academic Editor: Cherng-Yuan Lin

Received: 16 December 2022
Revised: 22 January 2023
Accepted: 27 January 2023
Published: 31 January 2023

1. Introduction

Hydrogen is an environmentally friendly fuel that has a very high calorific value, which is about 143 MJ/kg. With the development of various technologies and the emphasis on environmental protection, the trend of using liquid hydrogen as an alternative fuel for aviation kerosene is becoming more and more evident in recent years. Major international aircraft and aero engine manufacturers have successively put forward corresponding hydrogen-fueled aviation concepts and configurations [1,2]. The research on hydrogen-fueled aero engines has also gradually enriched. For the advanced hydrogen-fueled aero engines currently under research and development, most of the modifications are in the combustor and control system. In the design process of the control system of a hydrogen-fueled aero engine, both the design of the control law and the design of the safety protection system need to be based on the engine performance model. Based on these requirements, this paper mainly focuses on the modeling and performance simulation of the nonlinear model [3–5] of the hydrogen-fueled aero engine.

As early as the 1950s, research on hydrogen-fueled aero engines was performed by both Pratt & Whitney and the Former Soviet Union [6–8], which showed that the main changes in a hydrogen-fueled engine, compared with a kerosene-fueled engine, would be the combustor, control system, and thermal management system. As the basis for engine

system design and optimization, especially to control system design and development, the modeling and simulation of hydrogen-fueled engines with different configurations by different tools were explored.

In 2006, Fredrik Haglind [9] constructed a hydrogen-fueled engine model based on V2527-a5 using the software TURBOMATCH [10] developed by the Department of Power and Propulsion of Cranfield University, mainly to calculate hydrogen-fueled engine emissions and performance at some operating points. The model was developed based on the iterative method. In 2009, Daniel C. Villarreal [11] established a turboshaft hydrogen-fueled engine model also by the iterative method and used it to carry out the first iteration of controller design. The model was calibrated using experiment test data, in which traditional aviation kerosene was replaced with hydrogen, but the liquid hydrogen heat exchange and reasonable configuration of a hydrogen-fueled engine was not considered. In 2019, Emmanuel O. Osigwe [12] developed a multipurpose simulation tool (GT-ACYSS) which is based on component-level modeling and using the iterative method, and it can be used for steady-state performance simulation for closed-cycle gas turbines. The code was used in 2021 to analyze the performance and evaluate the creep life and exergy [13] of a hydrogen-fueled three-rotor turbofan engine. In 2022, Hamidreza Abedi [14] established a reference model of an engine operating with Jet A by matching the performance and dimensions of the 2020 short–medium range (SMR) turbofan engine technology and changed it to a hydrogen-fueled engine by referring to the technology proposed by the project ENABLEH2, and it was used to analyze the performance of the proposed heat exchanger.

As can be seen from the survey above, a dynamic model considering the reasonable configuration of hydrogen-fueled aero engines is lacking. The modeling of hydrogen-fueled aero engines with advanced configuration is used for steady-state performance analysis, while the current transient modeling used for control system design simply changes the fuel characteristics. The transient models of advanced configuration hydrogen-fueled aero engines are rarely found in the public domain. Therefore, this paper will mainly focus on the transient modeling of advanced hydrogen-fueled aero engines, which includes the wet NOx reduction combustor and the heat exchange system. Moreover, a rapid evaluation method of the NOx emission index is proposed, and a comparison between a conventional engine configuration and two hydrogen-fueled engine configurations is made in terms of engine-specific fuel consumption (SFC), turbine entry temperature (TET), and NOx emissions level.

This paper is organized as follow: Section 2 presents two structures and some modeling challenges of hydrogen-fueled aero engines. Section 3 deals with the methodology of the hydrogen-fueled aero engine modeling. Section 4 presents the simulation results of the conventional baseline engine model and the two hydrogen-fueled engine models. Finally, the paper ends with conclusions and prospects.

2. Modeling Challenges for Hydrogen-Fueled Aero Engines

Because of the consideration of environmental factors and energy factors, as well as the many advantages of hydrogen energy, major international organizations and companies have published research plans and schemes for hydrogen-fueled aircrafts or engines, respectively. Among them, the European ENABLEH2 project scheme and the Pratt & Whitney HySIITE project scheme are the most typical. The configuration of the two schemes mentioned above is introduced in this part to illustrate the differences between advanced hydrogen-fueled aero engine configurations and traditional engines, as well as analyze the modeling challenges for hydrogen-fueled aero engines.

2.1. Hydrogen-Fueled Aero Engine Configurations

2.1.1. ENABLEH2 Configuration

The configuration scheme proposed by the ENABLEH2 project for the hydrogen-fueled turbofan engine is shown in Figure 1. Firstly, the liquid hydrogen enters the fuel transmission pipeline from the 22 K liquid hydrogen storage tank, and it enters the precooler

between the fan and the low-pressure compressor for heat exchange at a temperature of 24 K. After passing through the heat exchanger, the hydrogen temperature is heated to 228 K, and the liquid is transformed into gas, then it enters the intercooler between the low-pressure compressor and the high-pressure compressor for heat exchange, and it is heated to 307 K. Then, the hydrogen is heated to 324 K by the cooling air from the high-pressure compressor to the high-pressure turbine entry. Finally, the hydrogen is heated by the nozzle recuperator and sent to the combustor for combustion at a temperature of 700 K [1].

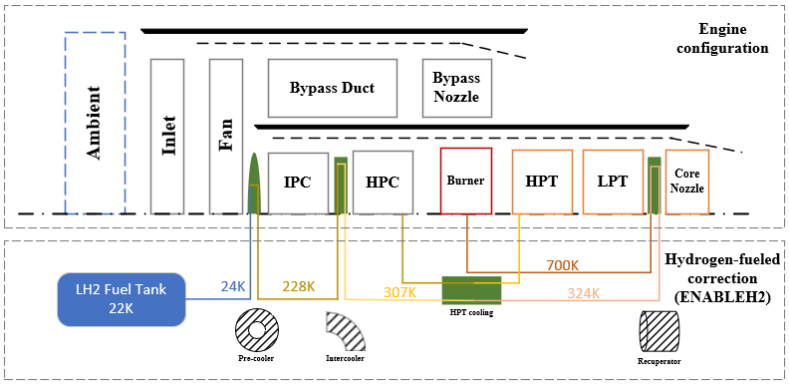

Figure 1. Configuration of hydrogen-fueled turbofan engine proposed by European ENABLEH2 project [1].

This scheme aims to use liquid hydrogen as the huge heat sink of the whole engine, which includes four heat exchangers. While heating the hydrogen to 700 K, it completes the steps of precooling, intercooling, and regeneration. This plays a great role in the thermal cycle efficiency of the whole system and in reducing the temperature of the combustor. It cools different parts of the aero engine and is conducive to improving the durability and efficiency of engine parts. At the same time, the exothermic combustion of hydrogen fuel is increased, which is a set of efficient and comprehensive hydrogen-fueled configurations. However, the disadvantage is that this scheme will add multiple heat exchangers of different forms, and there is a coupling relationship between the cooling and fuel systems, because the exchanged heat depends on fuel flow, which makes the system more complex and more difficult to model.

2.1.2. HySIITE Configuration

In April 2022, the HySIITE project of Pratt & Whitney obtained the support of USD 3.8 million from the US Department of Energy (DOE) and announced the hydrogen–steam injection intercooled engine scheme of the project, as shown in Figure 2.

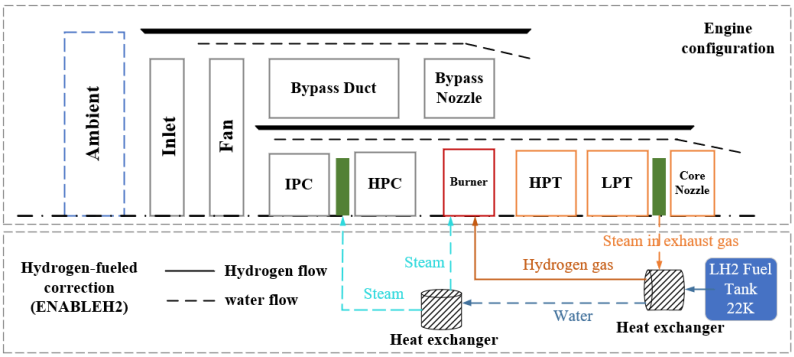

Figure 2. Configuration of hydrogen-fueled turbofan engine proposed by P&W's HySIITE project [2].

Different from the ENABLEH2 project scheme, in the HySIITE scheme, hydrogen only exchanges heat with the exhaust gas in the nozzle. In addition to heating hydrogen,

the main purpose is to collect the only product of hydrogen combustion in the exhaust gas–water steam. The cooled water is injected into the intercooler and combustor in the form of steam after heat exchange with other components that need to be cooled, so as to reduce the flame temperature and inhibit NOx emission. At the same time, the liquid hydrogen heated by the exhaust gas evaporates into hydrogen gas and is injected into the combustor for combustion [2]. The steam injection technology may have the problem of the oxidation of the combustor, but this technology has been developed and applied in the ground gas turbine for many years and has not been found to have a significant impact on the life of the combustor. From the development history of ground gas turbine technology, the technical difficulty of steam injection is relatively lower than that of other low-emission technologies, and it is more mature in engineering.

This scheme has a simple structure and is easier to realize than the scheme of ENABLEH2. The wet NOx reduction technology, which uses steam injection into the combustor to reduce NOx emissions, has been mature and widely used in gas turbines. However, in this scheme, all hydrogen is heat-exchanged at the nozzle. If the temperature of the hydrogen injected into the combustor is the same as that in the ENABLEH2 scheme, it will inevitably cause greater thrust loss.

2.2. Analysis of Modeling Challenges

Because of some phase and combustion characteristics of hydrogen, the actual hydrogen combustion thermodynamic cycle is different from that of the conventional engine. In the HySIITE and ENABLEH2 schemes, although the configurations are different, intercooling and regeneration are added in both schemes. The air between the compressor is cooled, and the heat of the exhaust gas is used to warm the fuel, which will help to improve the thermal cycle efficiency and alleviate the high temperature caused by hydrogen combustion. The change in thermal cycle also means a change in cooling system in the engine structure, which is usually realized by adding heat exchangers. In the European ENABLEH2 scheme, four heat exchangers are added between the fan and the low-pressure compressor, between the low-pressure compressor and the high-pressure compressor, on the bleed pipe behind the high-pressure compressor, and at the core nozzle. In the latest configuration released by Pratt & Whitney's HySIITE program, the heat exchanger from the core nozzle, the heat exchanger with the aircraft system, and several water spray cooling devices are also added. This also makes it necessary to add multiple heat exchange structures when establishing the nonlinear model, which makes the model more complex. If the conventional modeling method based on Newton–Raphson iteration [15] is used, the complex configuration of the hydrogen-fueled aero engine will make the algorithm difficult to converge, and the real-time performance cannot meet the verification requirements of the control algorithm.

At the same time, the heat exchanger components in the hydrogen-fueled engine are different from those in the conventional engine. Especially in the configuration scheme of ENABLEH2, all heat exchangers use hydrogen for cooling. However, the mass flow rate of hydrogen varies with the change in the thrust demand, which will lead to the change in the exchanged heat of the aero engine. Thus, the fluctuation of the thrust of the aero engine is caused, which shows the strong coupling between hydrogen fuel cooling and hydrogen fuel control, bringing challenges to the modeling and control of the hydrogen-fueled aero engine.

In addition, the most challenging model module for the hydrogen-fueled aero engine is the modeling of the hydrogen burning combustor. In addition to the different fuel characteristics, it also has the characteristics of rapid flame propagation, leading to the change in aero engine dynamic characteristics, low-emission combustor design such as water spray/steam injection, NOx emission assessment, etc. The dynamic model is required to verify the relevant functions of the hydrogen-fueled control algorithm.

Based on the challenges of the above hydrogen-fueled engine modeling and the requirements for the verification of the hydrogen-fueled control algorithm, this paper aims to explore the modeling method of a hydrogen-fueled aero engine and develop a stable and

dynamic model of hydrogen-fueled aero engine that can be used for subsequent control algorithm verification, as well as simulate and compare the existing open configurations.

3. Nonlinear Models of Hydrogen-Fueled Aero Engines

According to two published configuration schemes [1,2], based on an original model of the CF6 engine, the hydrogen-fueled engines are modeled in this part. The advanced hydrogen-fueled engines have a more complex structure than the traditional engine, with a problem of multisystem coupling, which poses a higher challenge to the real-time performance of the engine model. If the iterative method is used to solve the hydrogen-fueled engine model, there may be a situation that the calculation process may be stuck due to nonconvergence. Therefore, the hydrogen-fueled aero engine model in this paper is developed by the noniterative modeling method—volume dynamics modeling. As referred to in references [4,16–18], in volume dynamics modeling, a volume element is inserted between each pair of engine modules, allowing for the mass and energy storages which give rise to pressure and temperature dynamics, respectively.

3.1. Modeling of General Aero Engine Component

3.1.1. Environment and Inlet Compression

The standard atmospheric model is adopted for the inlet. The flight altitude H, flight Mach number Ma, and the total pressure recovery coefficient of the inlet σ_i are input. Firstly, the atmospheric temperature Ts_0 and atmospheric pressure Ps_0 are calculated through the altitude:

$$T_{s0} = \begin{cases} 288.15 - 6.5H & H \leq 11 \text{ km} \\ 216.65 & H > 11 \text{ km} \end{cases} \tag{1}$$

$$P_{s0} = \begin{cases} 101.325 \times (1 - H/44.308)^{5.2553} & H \leq 11 \text{ km} \\ 22.7\text{e}^{\frac{11-H}{6.338}} & H > 11 \text{ km} \end{cases} \tag{2}$$

Then, calculate the total temperature T_1 and total pressure P_1 at the inlet according to the flight Mach number:

$$T_1 = T_{s0}\left(1 + 0.2\text{Ma}^2\right) \tag{3}$$

$$P_1 = P_{s0}\left(1 + 0.2\text{Ma}^2\right)^{3.5} \tag{4}$$

The total temperature T_2 and pressure P_2 at the inlet exit can be obtained:

$$T_2 = T_1, P_2 = \sigma_i P_1 \tag{5}$$

3.1.2. Compression System

The basic idea for compression components is to interpolate the corrected flow and the isentropic efficiency of the compression components in the engine compressor map through the pressure ratio π_c and the correct speed:

$$(W_{ci_{cor}}, \eta_c) = f_{\text{compressor}}\left(n_{cor}, \pi_c\right) \tag{6}$$

where W represents the air mass flow rate, μ represents the adiabatic efficiency, n_{cor} represents the relative rotational speed, π represents the pressure ratio, subscript ci stands for compressor inlet, c stands for compressor, and cor stands for the corrected parameter. The calculation parameters of the later components used are introduced through the "Memory" module.

In the baseline engine model, there is no intercooling heat exchange device, but in the hydrogen-fueled engine configuration, the heat exchangers model will be added, which is described in detail in subsequent parts.

Two volumes will be inserted between the low-pressure compressor and the high-pressure compressor, including the pressure dynamics caused by the mass storage effect and the fast temperature dynamics caused by the energy storage [4]:

$$\dot{T}_{co} = \left(\frac{RT_{co}}{c_v P_{co} V}\right)(\dot{w}_{ci} h_{ci} - \dot{w}_{co} h_{co} + \dot{q}) - \left(\frac{RT_{co}{}^2}{P_{co} V}\right)\dot{w} \tag{7}$$

$$\dot{P}_{co} = (\rho R)\dot{T}_{co} + \left(\frac{RT_{co}}{V}\right)\dot{w} \tag{8}$$

where the subscript *co* represents the compressor outlet. c_v is the specific constant volume heat capacity, $\dot{w}$, $\dot{T}$, $\dot{P}$, respectively, stand for the change rate of the air mass flow rate, temperature, and pressure of the volume. h, ρ is the specific enthalpy and density of the air in volume. R is the gas constant, V represents the volume of the volume, and subscript *co* stands for compressor outlet. In the Equation (7), $\dot{q}$ is the thermal conductivity, belonging to slow temperature dynamics.The slow temperature dynamics are neglected in this work because the dynamics caused by metal-heating (or heat-soak) effects are very slow compared with those caused by the direct thermodynamic effects [4]; the heat conducted by metal has little change in a short period of time. Additionally, the influence of $\dot{q}$ is not considered in this study, as well as in most of the transient modeling using the volume dynamics modeling method in the industry [16,18] .

3.1.3. Turbine Expansion

The baseline model includes two expansion turbines, a high-pressure turbine and a low-pressure turbine. The gas works on the two turbines, and the output torque is transmitted to the compressors through the shafts. Similar to the compression components, the relationship among the pressure drop ratio, corrected speed, corrected flow, and isentropic efficiency of the turbine will correspond to the engine turbine map. The corrected flow and isentropic efficiency will be interpolated by the corrected speed and pressure drop, and then other parameters are calculated:

$$(W_{ti_{cor}}, \eta_t) = f_{\text{turbine}}\,(n_{cor}, \pi_t) \tag{9}$$

where the subscript *ti* represents turbine inlet, and *t* represents turbine. A volume is added after the high-pressure turbine and low-pressure turbine, respectively; the mass equation and energy equation are also used.

Two cavities will be inserted behind the high-pressure turbine and low-pressure turbine.

3.1.4. Exhaust System

In the CF6 turbofan engine, there are two convergent nozzles—the core nozzle and the bypass duct nozzle. The modeling mechanism for them is the same. The convergent nozzle has three working states, subcritical, critical, and supercritical [19]. It can be judged by the relationship between the available pressure drop of the nozzle and the critical pressure ratio. The available pressure drop of the nozzle is the ratio of the outlet pressure of the nozzle to the atmospheric pressure. The calculation of the critical pressure ratio $\pi_{e,cr}$ is shown in Equation (10).

$$\pi_{e,cr} = \left(\frac{k+1}{2}\right)^{\frac{k}{k-1}} \tag{10}$$

where k is the specific heat ratio.

Then, the static pressure, aerodynamic function $\pi(\lambda)$, velocity coefficient λ, and flow function $q(\lambda)$ at the exit of the nozzle can be obtained. The mass flow rate and velocity of the nozzle can be calculated after being obtained from different working conditions:

$$W_{no} = K \cdot \frac{P_{no} A_{no} q(\lambda_{no})}{\sqrt{T_{ni}}} \tag{11}$$

$$v_{no} = \sigma_e \lambda_{no} \sqrt{\frac{2k}{k+1} \cdot RT_{ni}} \tag{12}$$

where v is the gas velocity, K is a constant and $K = \sqrt{k(2/(k+1))^{\frac{k+1}{k-1}}/R}$, A is the area, σ_e is the restitution coefficient, and λ is the velocity coefficient, and the subscript *no* represents the nozzle outlet, and the subscript *ni* represents the nozzle inlet.

3.1.5. Rotor Shaft

The rotor shaft part is modeled by the shaft dynamics equation, which is caused by the inertial effect, and the rotor acceleration is obtained from the torque difference between the compression part and the turbine:

$$\dot{n} = \frac{\left(\eta_N P_{\text{turbine}} - P_{\text{compressor}}\right)}{(\pi/30)^2 J_n n} \tag{13}$$

where μ_N is the mechanical efficiency of shaft power transmission, P is the power output or consumption of turbomachinery, J_n is the moment of inertia of engine shaft, n is the rotor speed, and $\dot{n}$ is the rotor speed acceleration; the π here is the circular constant.

3.2. Modeling of Hydrogen-Fueled Components

3.2.1. Combustor

In the combustor of the baseline engine model, the general combustor modeling method is adopted [16], and the calculation accuracy is required to be high, so the simplified volumetric dynamic equation is not adopted, and the specific form of the energy equation is

$$\dot{T}_{como} = \frac{1}{\rho_{como} D_g} \cdot \left[W_f \cdot \left(\eta_{com} \cdot H_u + h_f - \frac{h_{como}}{k_{como}} \right) + W_{comi} \cdot \left(h_{comi} - \frac{h_{como}}{k_{como}} \right) - W_{como} \cdot (k_{como} - 1) \frac{h_{como}}{k_{como}} - Q_{steam} \right] \tag{14}$$

$$D_g = \frac{d\left(\frac{h_{como}}{k_{como}}\right)}{dT_{como}} \tag{15}$$

where W_f is the fuel flow rate, μ_{com} is the combustion efficiency of the combustor, and Hu is the low heat value of the fuel. h is the specific enthalpy, and k is the adiabatic index. The subscript f represents the fuel, and Q_{steam} is the heat carried by steam injection, which is described in the following part. The specific form of the mass equation is

$$\dot{P}_{como} = \frac{R \cdot T_{como}}{V} \cdot \left(W_f + \Delta W_{com} \right) + P_{como} \cdot \frac{\dot{T}_{como}}{T_{como}} \tag{16}$$

where subscript *como* represents the combustor outlet, and subscript *comi* represents the combustor inlet.

However, in the hydrogen-fueled engine, the high-temperature flame generated by hydrogen combustion will bring high NOx emissions. Usually, the method of injecting steam into the combustor will be used to reduce the temperature of the flame and to reduce NOx emissions. This technology has been developed in the automotive engine and ground gas turbine [20–23]. This technology is also used in the hydrogen-fueled engine scheme announced by the HySIITE program. Thus, this part also considers the modeling of this technology in the model, that is, to simulate the impact of steam injection on the combustor

temperature calculation. At the same time, the NOx emission index model is also added to the model to calculate NOx emissions.

3.2.2. Effect of Steam Injection on the Combustor

In the HySIITE scheme, after heat exchange between exhaust gas and hydrogen, steam will be recovered and injected into the combustor to decrease the combustion temperature to inhibit the generation of NOx.

Assuming that steam is injected into the combustion chamber at an initial state of 100 °C and finally reaches the same temperature as the gas. According to the principle of engineering thermodynamics [24], the heat absorbed by water vapor in this process is calculated by the following equation:

$$Q_{steam} = W_{steam} \times \left[T_{steam} \times \bar{C}p_{0\_100} - T_{como} \times \bar{C}p_{0\_T_{como}}\right] \tag{17}$$

where W_{steam} presents the steam flow rate, $\bar{C}p_{0\_100}$ presents the average specific heat capacity of water at $t_0 = 0$ °C, $t_f = 100$ °C, $\bar{C}p_{0\_T_{como}}$ presents the average specific heat capacity of water at $t_0 = 0$ °C, $t_f = T_4$, and the average specific heat capacity can be obtained from the thermodynamic property table [24]:

$$\bar{C}p_{0-t_f} = f\left(t_f\right) \tag{18}$$

3.2.3. Modeling of Heat Exchanger

Since the model's constructed in this paper is mainly used for the design of the control system, and the continuity of transient calculation is required, the heat exchanger will consider the heat exchange process from the perspective of zero-dimensional modeling.

Heat exchanger modeling is mainly based on the principle of enthalpy increase or enthalpy decrease in the heat exchange medium. When hydrogen and air exchange heat, there is

$$\dot{w}_{H_2} \cdot \int_{T_{H_2\,\text{in}}}^{T_{H_2\,\text{out}}} C_{P_{H2}} dT = \dot{w}_{\text{air}} \cdot \int_{T_{\text{air in}}}^{T_{\text{air out}}} C_{P_{\text{air}}}\, dT \tag{19}$$

Under the assumption of constant specific heat, the above formula can be written as

$$Q_{H_2} = \dot{w}_{H_2} \cdot Cp \cdot \Delta T = \dot{w}_{\text{air}} \cdot \eta_{HE} \cdot (H_{\text{air out}} - H_{\text{air in}}) \tag{20}$$

where Q represents the total heat exchange, $\dot{m}$ represents the mass flow rate, T represents the temperature, C_p represents the specific heat at constant pressure, μ_{HE} presents the heat exchanger efficiency, and H represents the enthalpy of the heat exchange medium. For the same medium, there is a one-to-one correspondence between temperature and enthalpy:

$$H = f(T), T = f(H) \tag{21}$$

As modeling of the hydrogen fuel pipeline is not involved in this paper, the change in gas pressure in the heat exchanger is not considered.

3.3. NOx Emission Assessment

Many factors affect NOx emission, among which temperature is the most critical. Due to high flame temperature, if no cooling strategy is adopted, the NOx emission of hydrogen combustion will be several times higher than that of traditional aviation kerosene combustion [25]. Therefore, NOx emission is also an important technical index of the hydrogen-fueled engine. In the control of the hydrogen-fueled aero engine, low emission control is also a key technology.

As shown in Figure 3, for the same engine, the corrected fuel flow rate has a one-to-one correspondence with the reference NOx emission index [26], and the corrected fuel flow rate also has a unique functional relationship with the combustor outlet temperature. Therefore,

the relationship between the combustor outlet temperature and the NOx emission index is shown in Figure 4.

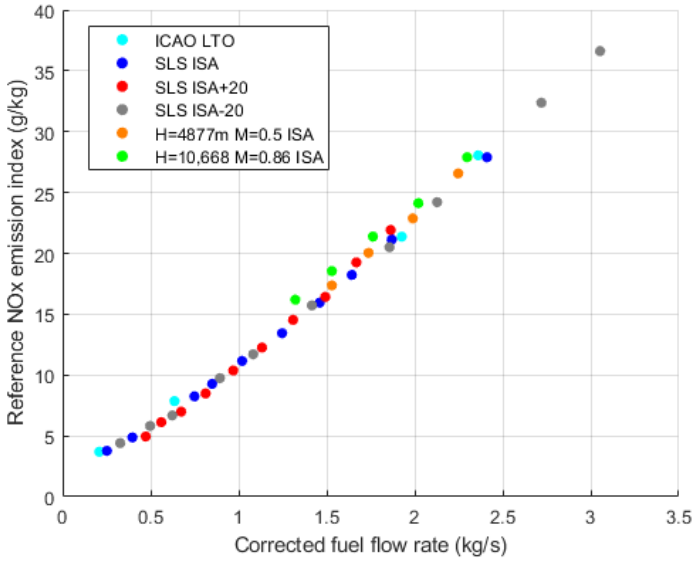

Figure 3. Relationship between CF6 engine corrected fuel flow rate and reference NOx emission index [26].

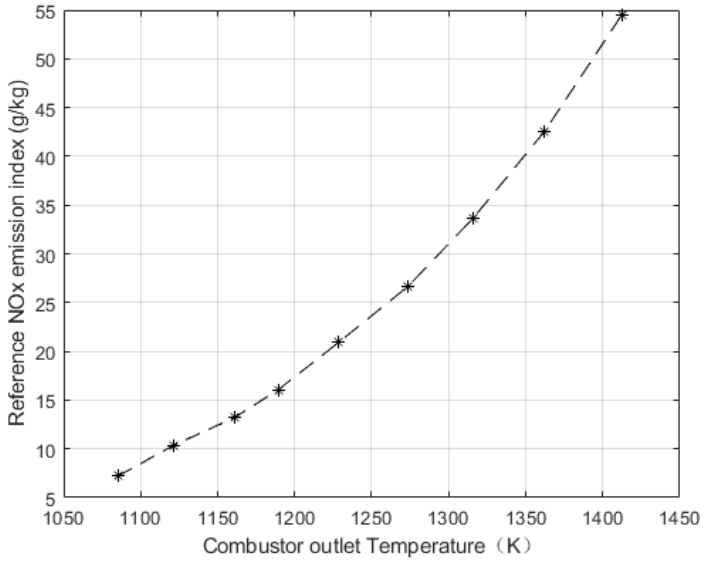

Figure 4. Relationship between CF6 engine combustor outlet temperature and reference NOx emission index.

The actual NOx emission index at the operating point has the following relationship with the reference NOx emission index [26]:

$$\frac{EI_{NOx}}{EI_{NOx_{ref}}} = \frac{EI_{NOx}}{EI_{NOx_{ref}}} = \delta_t^a \cdot \theta_t^b \tag{22}$$

where

$$\delta_t = \frac{P_1}{P_{amb}}, \theta_t = \frac{T_1}{T_{amb}} \tag{23}$$

After the reference NOx emission index is obtained from the combustor outlet temperature, the actual NOx emission index can be calculated. In the CF6 engine, a is taken as 0.4, and b is taken as 3 [27]. In this paper, in order to compare the NOx emission under the

same thrust, the specific NOx emission index is defined, that is, the index under the unit thrust, which is introduced in the simulation results part.

4. Performance Analysis of Advanced Hydrogen-Fueled Aero Engine

Three transient models for the kerosene-fueled CF6 (the baseline engine) and the two hydrogen-fueled engines (ENABLEH2 and HySIITE) are constructed by integrating the general engine component models with the specific hydrogen-related component models. Simulation is carried out over the same flight envelope, while the same maximum thrust is assumed, and the performance indices, SFC, TET, and the NOx emission level are calculated and compared for those three types of engines.

To make the two schemes as similar as possible in terms of conditions, except the configuration, so as to facilitate the comparison of the performance differences of different engine schemes, the following assumptions are made in the simulation:

1. Hydrogen fuel needs to heated from 24 K at the outlet of the hydrogen storage tank to 700 K and then be injected into the combustor in both the ENABLEH2 scheme and HySIITE scheme.
2. In the HySIITE scheme, the flow of steam injected into the combustion chamber is 3% of the gas flow at the outlet of the engine turbine, and steam is injected into the combustor at 100 °C and finally reaches the same temperature as the combustor.
3. Under the same operating point, the fuel flow command corresponding to the PLA is only one proportion coefficient different between the kerosene-fueled model and the hydrogen-fueled model.

In addition, the steam mass flow rate and temperature in assumption 2 are adjustable variables, which can be optimized when the engine is designed or controlled. In this paper, the parameters mentioned above are assumed to be constant values to validate the hydrogen-fueled engine model. In the simulation, the command changes in PLA , altitude, and Mach number are shown in Figures 5 and 6.

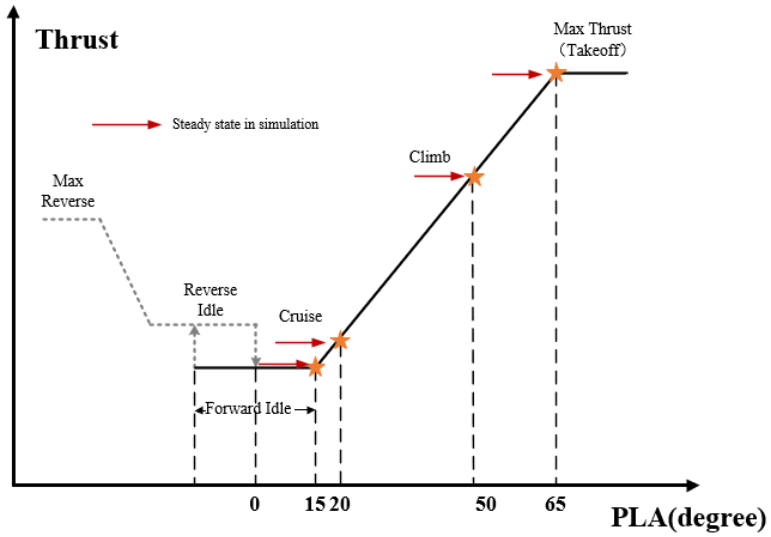

Figure 5. PLA command Interpolation curve.

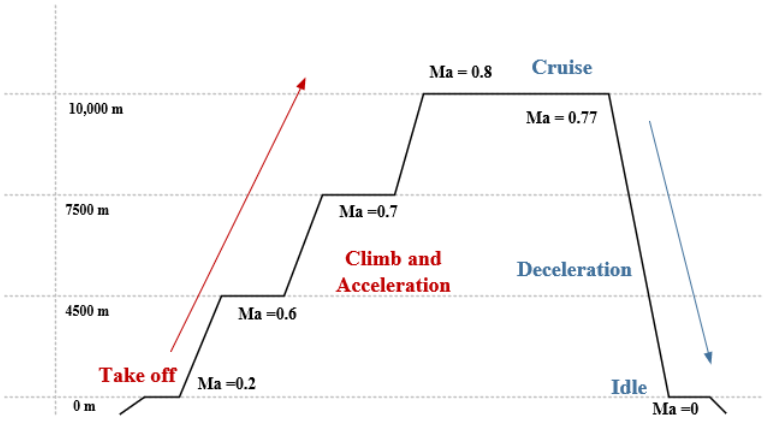

Figure 6. Schematic curve of altitude and Mach number.

The flight envelope is divided into seven steady states in the simulation: two take-off states, three climb states, cruise states, and idle states. The steady-state simulation commands are shown in Table 1:

Table 1. Simulation status description.

State	Takeoff 1	Takeoff 2	Climb 1	Climb 2	Climb 3	Cruise	Idle
Height (m)	0	0	4500	7500	10,000	10,000	0
Mach number	0	0.2	0.6	0.7	0.8	0.77	0
PLA (degree)	65	50	50	50	50	20	15

The simulation was carried out by the Simulink tool. Simulink is a MATLAB-based graphical programming environment for modeling, which is widely used to simulate and analyze multidomain dynamical systems [28].

The simulation results under the above simulation settings are analyzed in this part. First, compare the trend of the three key parameters (fuel flow, SFC, and TET) in the entire flight envelope. Then, performance parameters such as cross-section parameters (including cross-section temperature and pressure), thrust, SFC, TET, intake mass flow rate, and exhaust gas speed under the three key states are analyzed in detail. The performance differences between the advanced hydrogen-fueled aero engine configuration and the traditional configuration are compared, as well as those between different hydrogen-fueled configurations. The the trend of the steady-state result of the model is verified. Finally, the simulation is carried out on the HIL platform to verify that the dynamic model can be used for subsequent controller design and HIL experimental verification.

4.1. Analysis of Key Performance Parameters under the Same Maximum Thrust

The thrust comparison in the simulation results is shown in Figure 7. Three configurations have similar thrust and thrust changes, as shown in Figure 7a.

It can be seen in Figure 7a that, under the same maximum thrust, with the increase in altitude and Mach number, the thrust of the ENABLEH2 scheme in other states will gradually be slightly higher than that of the baseline engine, while the thrust of the HySIITE scheme is the highest. This is caused by the coupling of heat exchange and fuel control due to the nonrecoverability of hydrogen. The heat exchange at the core nozzle leads to the change in the gas pressure, resulting in thrust loss. Under the small thrust state, the reduction in hydrogen flow causes the heat exchange decrease, which makes the pressure drop of the core nozzle reduce, and the thrust loss also decreases. Therefore, under the same maximum thrust state, the thrust in other states is different. The greater difference the HySIITE scheme has is because, in this scheme, the heat of gasification and temperature

rise of hydrogen will all be provided by the exhaust gas waste heat of the core nozzle, so the thrust loss is greater.

Note in the local thrust curve (Figure 7b) that the thrust of the HySIITE scheme fluctuates during the takeoff state transition. This is due to the coupling of the fuel and cooling systems. The change in the Mach number and the fuel flow causes the change in the inlet airflow, so that the steam injection amount of the combustion chamber in the HySIITE scheme also changes with the temperature of the combustion chamber changes, resulting in the thrust fluctuation. However, as the calculation continues, it finally convergences to a new steady equilibrium state. It can also be seen from here that the volume dynamics model will not be interrupted due to abnormal calculation at a certain point and has good real-time performance.

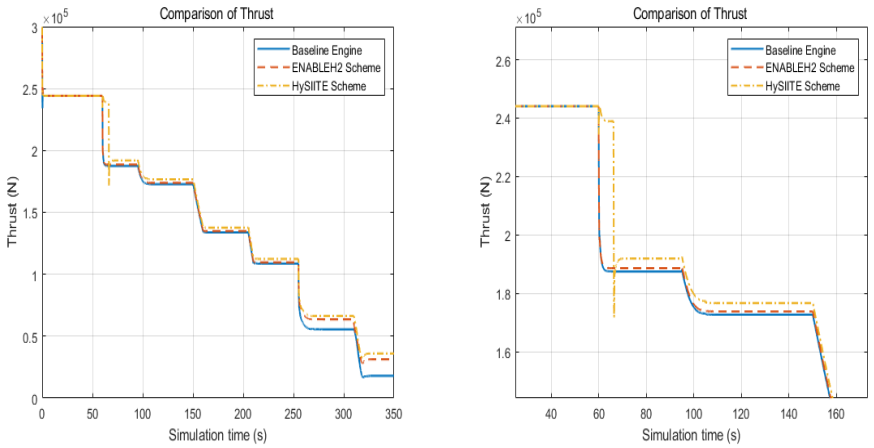

Figure 7. Thrust comparison of baseline engine, ENABLEH2 scheme, and HySIITE scheme: (**a**) thrust curve under full flight envelope; (**b**) local thrust curve.

One of the great advantages of hydrogen as aviation fuel is its high LHV (Low Heat Value), 3–4 times that of kerosene. The simulation results of fuel flow rate and specific fuel consumption (SFC) of the three configurations are shown in Figure 8a,b. According to the mass flow rate, the fuel flow rate and SFC of the two hydrogen-fueled engines are significantly lower than those of the baseline engine. In other words, under the condition of mature liquid hydrogen storage technology, the same takeoff weight of hydrogen-fueled civil aviation means higher passenger capacity than kerosene-fueled aircraft. Because of the influence of a large amount of heat exchange in the nozzle of the HySIITE scheme, the thrust loss is higher than that of the ENABLEH2 scheme to achieve the same maximum thrust; the HySIITE scheme consumes more fuel. Compared with the HySIITE scheme, the average SFC of the ENABLEH2 scheme can be decreased by 6.64%. Therefore, the ENABLEH2 scheme has better economy in terms of SFC indicators.

In the future, with the maturity of technologies related to the hydrogen energy ecosystem, the cost of hydrogen production and hydrogen transportation will decrease. This means that the economy of hydrogen-fueled engines will be greatly improved compared with conventional engines. This is also one of the important reasons why major economies, aircraft, and engine manufacturers attach great importance to the development of hydrogen powerplants.

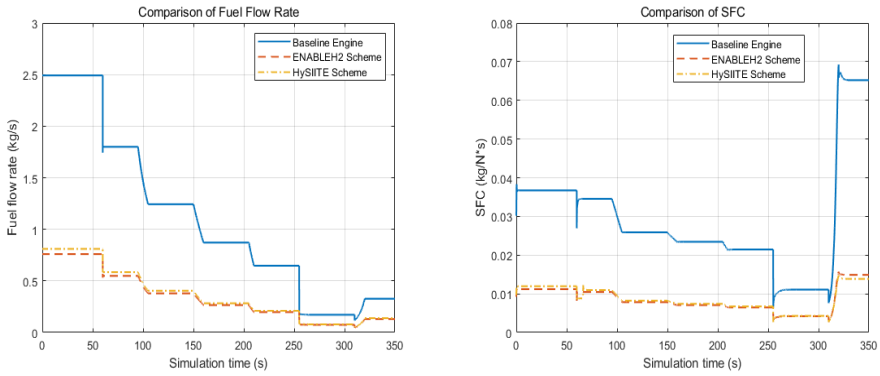

Figure 8. SFC comparison of baseline engine, ENABLEH2 scheme, and HySIITE scheme. (**a**) Comparison of fuel flow rate; (**b**) comparison of SFC.

In the engine performance analysis, the turbine entry temperature affects the service life of the turbine hot-end components and the safety of the engine. Without cooling treatment, the combustion temperature of the hydrogen-fueled engine will be higher than that of the conventional kerosene-fueled engine, resulting in higher NOx emissions and lower service life of the hot-end components.

A large number of heat exchangers are used in the schemes announced by the ENABLEH2 and HySIITE projects. In the European ENABLEH2 project scheme, hydrogen is used as a huge heat sink to cool the compressor, core nozzle, and other places. The HySIITE project of Pratt & Whitney collects the water vapor at the core nozzle and injects it into the compressor interstage and combustor for cooling. The simulation results of turbine entry temperature for the three configurations are shown in Figure 9.

From the simulation results, it can be seen that the advanced hydrogen-fueled engine configuration has a good effect on reducing the TET in the takeoff and climb process. In these two states, the TET is high, which has a great impact on the life and safety of the hot-end components. This shows that the advanced hydrogen-fueled engine configuration can effectively improve the life and safety of the hot-end components of the engine. This is in accordance with the actual situation, because the advanced hydrogen-fueled engine configuration can use hydrogen fuel to reduce the overall temperature of the engine, and the water vapor generated by hydrogen combustion has a large specific heat capacity, which can absorb more heat in the combustion chamber.

In the states that require low thrust , the TET of the ENABLEH2 scheme is higher than that of the baseline engine, while the TET of the HySIITE scheme is lower than that of the baseline engine. This is because the hydrogen fuel delivery is less in the case of a small PLA (Power Lever Angle) situation, and the cooling effect of the ENABLEH2 scheme on the engine is also reduced. In the HySIITE scheme, there is a device that directly injects steam into the combustion chamber for cooling, so the TET can still be effectively reduced in the case of small hydrogen flow.

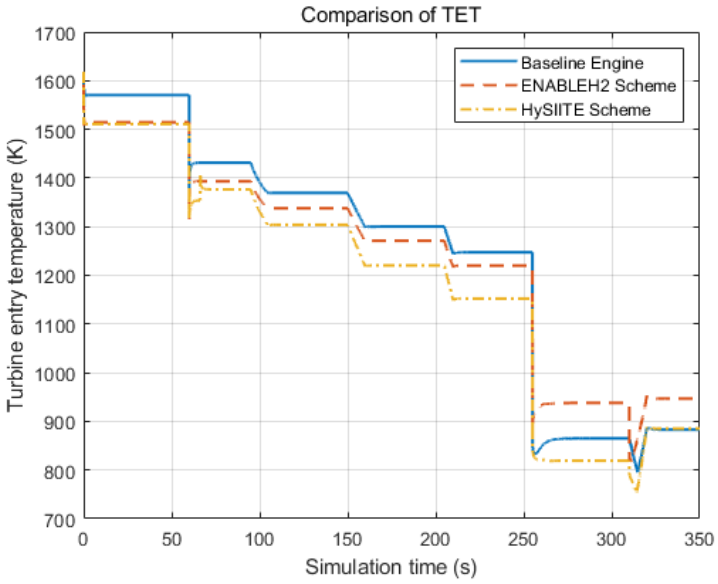

Figure 9. TET comparison of baseline engine, ENABLEH2 scheme, and HySIITE scheme.

4.2. Analysis of Performance Parameters under Key Operating Points

In addition to its high LHV, hydrogen fuel also has the most noteworthy advantage of environmental protection. If only hydrogen combustion is considered, its product is only water. Compared with various carbon and oxygen compounds produced by aviation kerosene combustion, hydrogen is completely environmentally friendly. However, its high-temperature combustion will also bring serious NOx emissions. Therefore, monitoring NOx emissions is also an issue that needs attention in the hydrogen-fueled engine model.

Under the simulation assumption in this paper, the maximum thrust is the same, and the thrust in other states may be different. In order to better analyze the NOx emission of each configuration under the same thrust, this paper introduces a new NOx emission index per unit thrust (specific NOx emission index) based on the NOx emission index [27], and its expression is as follows:

$$\hat{I}_{NO_x} = \frac{EI_{NO_x}}{F} \tag{24}$$

where $\hat{I}_{NO_x}$ is the specific NOx emission index, EI_{NO_x} is the NOx emission index, and F is the thrust of the engine.

The simulation results are shown in Figure 10.

As seen in Figure 10, the Specific NOx emission index of the advanced hydrogen-fueled aero engine is lower than that of the baseline engine under takeoff and idle conditions, that is, under the same thrust, the hydrogen-fueled aero engine has lower emissions. In the cruise state, the emission of the ENABLEH2 scheme is slightly higher than that of the baseline engine, which is caused by the reduction in the cooling capacity of the engine body due to the reduction in the fuel flow rate. This is because hydrogen combustion itself will emit more NOx than aviation kerosene combustion due to high combustion temperature; if no better cooling or low-pollution combustion measures are taken, the NOx emissions of hydrogen-fueled aero engines may be higher than traditional engines. The HySIITE scheme can still effectively reduce emission because of the steam injection in the combustor.The steam injection technology, which has been developed and applied in the ground gas turbine for many years, has not been found to have a significant impact on the life of the combustor [29]. The technical difficulty of steam injection is relatively lower than that of lean premixed combustion, and the design of steam injection technology is more mature in engineering [30,31]. Therefore, at present, the steam injection technology is the first choice of most hydrogen-fueled aero engine companies.

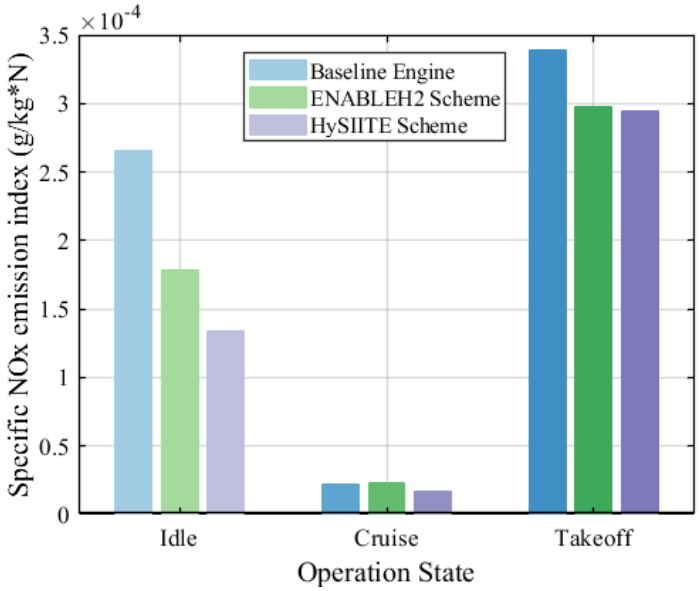

Figure 10. NOx emission comparison of the baseline engine, ENABLEH2 scheme, and HySIITE scheme at different operating points.

Through a configuration design and thermal management scheme, hydrogen-fueled engines can effectively inhibit NOx emission, among which the HySIITE configuration has the best inhibition effect on NOx, and the model also successfully reflects the low emission effect of wet NOx reduction technology that injects steam into the combustion chamber. In the idle and cruise states, the aircraft is in a relatively low power state, and the NOx emission of the hydrogen-fueled engine is not very different from that of the kerosene-fueled engine. Under the maximum thrust state, the emission advantages of the new hydrogen-fueled aero engine configuration can be observed.

Figure 11 is the pressure and temperature distribution diagram of each section under the three states of idle, cruise thrust, and takeoff. Section H refers to the ambient, section 2 refers to the inlet of the fan, section 2c refers to the inlet of the core compressor, section 3 refers to the outlet of the compressor, section 4 refers to the outlet of the combustion chamber, section 5 refers to the turbine outlet, and section 9 refers to the core nozzle outlet.

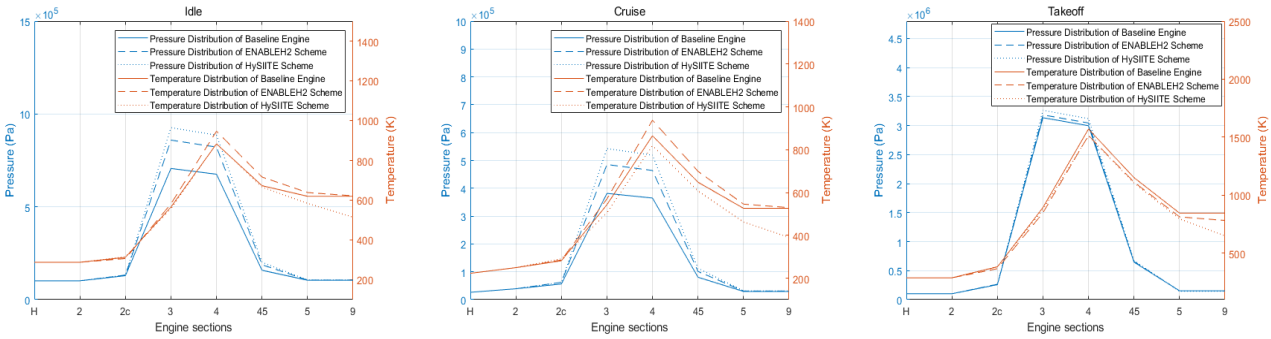

(**a**) (**b**) (**c**)

Figure 11. Comparison of temperature and pressure parameters of different engine sections: (**a**) temperature and pressure distribution at idle state; (**b**) temperature and pressure distribution at cruise state; and (**c**) temperatureand pressure distribution at takeoff state.

The reason why the temperature of the whole engine in the ENABLEH2 scheme is higher than that in the baseline engine and HySIITE scheme is that the cooling capacity of the ENABLEH2 scheme depends on the fuel flow, while the fuel flow is less in the small PLA state. In the takeoff state, which is the maximum thrust, the temperature of the whole

engine in both the ENABLEH2 scheme and the HySIITE scheme is lower than the baseline engine. The temperature in the HySIITE scheme before the combustion chamber is lower than that in the ENABLEH2 scheme, which is opposite after the combustion chamber. Due to the coupling between the cooling system and the fuel system of the hydrogen-fueled engine, the larger the fuel flow rate, the better the cooling effect of the hydrogen-fueled engine.

In terms of pressure distribution, the internal pressure of the hydrogen-fueled engine is higher than that of the baseline engine. It can also be seen from Figure 11 that the hydrogen-fueled engine has a higher pressure ratio. The core pressure ratios ($\pi_{core} = P_3/P_2$) of the three engines are shown in Table 2. The π_{core} of two hydrogen-fueled engine is higher than that of the baseline engine in the idle, cruise, and takeoff state. This is caused by the heat exchange in the compressor part of hydrogen-fueled aero engine.

Table 2. Simulation results of core pressure ratio of three configurations under different operating points.

	Idle	Cruise	Takeoff
Baseline	6.6677	9.3318	29.5893
ENABLEH2	8.1080	11.8650	30.0469
HySIITE	8.7429	13.2675	30.7973

At the same time, it can be seen that HySIITE has the best pressurization effect, but the temperature drop at the core nozzle is the most obvious, which means the thrust loss is the largest.

As for the overall thermal cycle efficiency, it was not calculated in this specific value. However, theoretically, the cycle efficiency of the new cycle with regenerative and intercooling added to the original cycle will be higher than that of the original cycle [24]. This means that the two hydrogen-fueled engine cycle schemes are beneficial to the overall thermal efficiency of the cycle.

Table 3 shows the simulation results of various parameters under the conditions of idle, cruise, and takeoff states. It can be seen that there is a relationship between air flow rate in all states: $W_{2HySIITE} > W_{2ENABLEH2} > W_{2baseline}$. This is because the lower temperature and higher pressure ratio inside the engine make the engine have a stronger flow capacity. The relationship between the core nozzle gas speed is $V_{cENABLEH2} > V_{cHySIITE} > V_{cbaseline}$ in idle and cruise states, which is due to the higher pressure ratio between the inside of the hydrogen-fueled engine and the atmosphere. In takeoff state, there is $V_{cbaseline} > V_{cENABLEH2} > V_{cHySIITE}$, which is due to the energy loss of the air flow caused by heat exchange at the core nozzle. According to the previous configuration description, the energy loss of HySIITE will be greater than that of the ENABLEH2 scheme. The bypass nozzle shows the $V_{bHySIITE} > V_{bENABLEH2} > V_{bbaseline}$, which is caused by the stronger flow capacity of hydrogen-fueled engine.

If the performance parameters of each configuration in the maximum state simulation are selected for analysis, it could be found that, under the same thrust in the maximum state, the hydrogen-fueled aero engine has a lower SFC than the conventional aero engine. Under the two typical configurations, the turbine entry temperature is also effectively reduced, which reflects the advantages of the hydrogen-fueled engine in economy, service life, and safety of hot-end components. These are also consistent with the expected results.

Since a large number of heat exchange devices reduces the temperature of the whole engine, the outlet temperature of the combustor decreases, and the wet NOx reduction combustor also reduces the emission of NOx. The simulation results show that the developed transient models can effectively reflect the hydrogen-burning, heat-exchanging, and NOx emission characteristics for hydrogen-fueled engines.

Table 3. Simulation results of key performance parameters of three configurations under different operating points.

	Idle			Cruise			Takeoff		
	Baseline	**ENABLEH2**	**HySIITE**	**Baseline**	**ENABLEH2**	**HySIITE**	**Baseline**	**ENABLEH2**	**HySIITE**
Thrust (N)	18,018.56	31,409.58	36,050.42	55,560.23	63,680.67	66,311.79	244,083.65	244,083.00	244,083.33
SFC (kg/N*s)	0.065233	0.014903	0.013847	0.011091	0.0041881	0.004289	0.036743	0.011202	0.011946
TET (K)	882.9705	946.741	885.0585	865.0847	937.8252	819.1171	1570.4416	1514.6401	1510.8762
W2 (kg/s)	215.2786	291.9656	316.113	239.9702	253.6827	258.5969	782.6713	783.8425	796.8
EI_NOx (g/kg)	6.5603	6.9754	6.588	1.6981	1.8853	1.322	82.8146	72.5875	71.9774
V_{core} (m/s)	104.6981	123.0769	113.4915	182.5949	221.5216	195.1924	434.7032	415.9945	358.28
V_{bypass} (m/s)	78.1037	106.3611	115.2574	258.7696	274.5102	280.0808	289.4343	289.876	294.7611
FAR	0.001516	0.00044536	0.0004386	0.0007133	0.00029203	0.00030551	0.0031829	0.00096895	0.0010165

4.3. Hardware in the Loop (HIL) Simulation Results

When designing the control law, it puts forward high real-time performance requirements of the model. Considering the complex configuration and multisystem coupling of advanced hydrogen-fueled aero engines, it is necessary to further verify the real-time performance of the model built in this paper to ensure the smooth operation of HIL simulation.

In this part, the HIL simulation of hydrogen-fueled engine models is carried out on the Speedgoat platform [32], the simulation step is 10 ms. This simulation can better reflect the real hardware operation, including electromagnetic interference, delay, and other phenomena. If a model will be used to verify the control algorithm on the HIL platform, it needs to ensure that the simulation results of the model on the HIL platform and the software platform are basically consistent. The HIL simulation results of hydrogen-fueled engine models are shown in Figures 12–14.

From the simulation results, the two hydrogen-fueled engine models achieved the consistency of software simulation and HIL simulation, but there will be some differences in the details of the operation process. As shown in Figure 14, HIL simulation results have certain time delays in signal transmission compared with software simulation, and the dynamic characteristics of signal response simulated on HIL are faster. These differences are inevitable in engineering implementation, and the implementation of the control algorithm cannot avoid the verification of the HIL simulation. The simulation results of this model on the HIL platform are consistent with the trend of software simulation and can reflect the real hardware operation, which can be used for the verification of subsequent simulation algorithms.

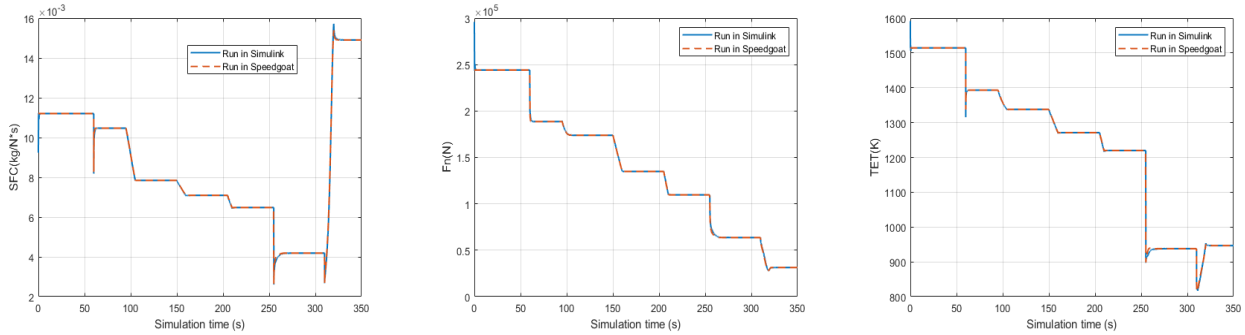

(**a**) (**b**) (**c**)

Figure 12. Comparison of HIL simulation and software simulation results of the ENABLEH2 scheme: (**a**) the SFC results; (**b**) the thrust results; and (**c**) the TET results.

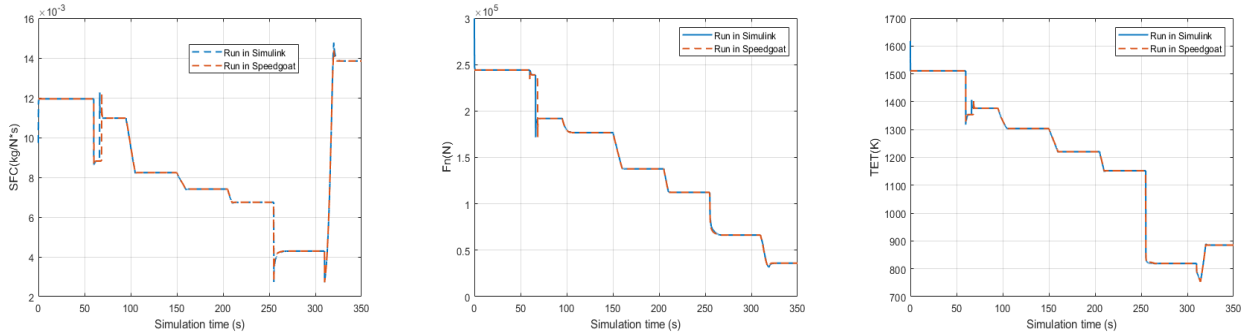

Figure 13. Comparison of HIL simulation and software simulation results of the HySIITE scheme: (**a**) the SFC results; (**b**) the thrust results; and (**c**) the TET results.

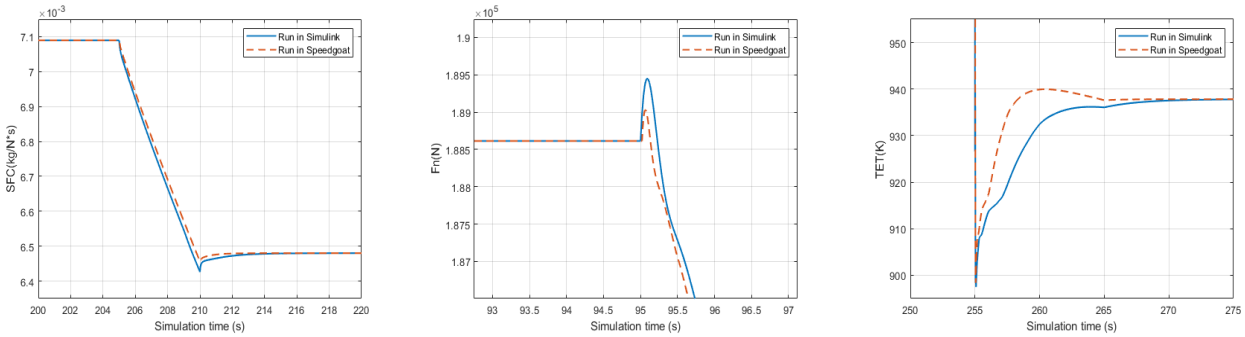

Figure 14. Comparison of HIL simulation and software simulation results of the ENABLEH2 scheme: (**a**) the SFC results; (**b**) the thrust results; and (**c**) the TET results.

5. Conclusions

Transient modeling and performance predication are critical to the advanced hydrogen-fueled engine system design and development. This paper explores the transient modeling method and does the performance analysis of the hydrogen-fueled engines, and the work concludes as follows:

- By referencing two hydrogen-fueled engine configurations from ENABLEH2 and HySIITE, replacing the typical turbofan engine CF6 with the hydrogen-burning combustor model, and integrating the heat exchanger, the water spray or steam injection system, and the NOx emission assessment of hydrogen-specific models, two component-based transient models that can simulate hydrogen-fueled aero engine characteristics are developed.
- The simulation results demonstrate the advantages of advanced hydrogen-fueled aero engines. Under the same maximum thrust condition, engine performance indices are compared among CF6, ENABLEH2, and HySIITE. The results show that the advanced configuration of the hydrogen-fueled engine can greatly reduce SFC, TET, and NOx. For example, at takeoff state, the advanced hydrogen-fueled engine can reduce the parameters mentioned above by about 68.5%, 3.7%, and 12.7%, respectively (mean value of two configurations).

It should be noted that one of the limitations in this study is the neglect of the thermal conductivity of metal, and the modeling work that considers these slow temperature dynamics is proposed to be conducted in the future. Other interesting work could also be carried out in the future: using more complex and accurate modeling methods, modeling the fuel pipeline, model calibration and validation, and control system design for hydrogen-fueled aero engines.

Author Contributions: Conceptualization, A.H.; Methodology, X.W. and A.H.; Software, X.W. and A.H.; Validation, X.W. and A.H.; Formal analysis, X.W.; Investigation, X.W.; Resources, A.H. and Z.H.; Data curation, X.W. and A.H.; Writing—original draft, X.W.; Writing—review & editing, Z.H.; Visualization, X.W.; Supervision, A.H. and Z.H.; Project administration, Z.H.; Funding acquisition, Z.H. All authors have read and agreed to the published version of the manuscript.

Funding: This research was funded by Tsinghua University Initiative Scientific Research Program, 20214180061. The APC was funded by Tsinghua University Initiative Scientific Research Program.

Institutional Review Board Statement: Not applicable.

Informed Consent Statement: Not applicable.

Data Availability Statement: Not applicable.

Conflicts of Interest: The authors declare no conflict of interest.

References

1. Bjorn's Corner: The Challenges of Hydrogen. Part 29. Gas Turbine Heat Management. Available online: https://leehamnews.com/2021/03/19/bjorns-corner-the-challenges-of-hydrogen-part-29-gas-turbine-heat-management/ (accessed on 5 June 2022).
2. Pratt Outlines Hydrogen Steam-Injection Engine Concept. Available online: https://aviationweek.com/special-topics/sustainability/pratt-outlines-hydrogen-steam-injection-engine-concept (accessed on 5 June 2022).
3. Wang, J.L. Aeroengine Nonlinear Modeling. In *Model-Based Nonlinear Control of Aeroengines*; Springer: Singapore, 2022; pp. 19–61.
4. Jaw, L.; Mattingly, J. *Aircraft Engine Controls*;American Institute of Aeronautics and Astronautics: New York, NY, USA, 2009.
5. Spang, T., III. Control of jet engines. *Control. Eng. Pract.* **1999**, *9*, 1043–1059.
6. Fulton, K. Cryogenic-Fueled Turbofans: Kuznetsov Bureau's pioneer work on LH2 and LNG dual-fuel engines. *Aircr. Eng. Aerosp. Technol.* **1993**, *65*, 8–11 . [CrossRef]
7. Brewer, G.D. *Hydrogen Aircraft Technology*, 1st ed.; CRC Press: Boca Raton, FL, USA, 1991; pp. 63–90.
8. Bukin, V.; Gimadiev, A.; Gangisetty, G. Correction of Dynamic Characteristics of SAR Cryogenic GTE on Consumption of Gasified Fuel. *IOP Conf. Ser. Mater. Sci. Eng.* **2018**, *302*, 012058. [CrossRef]
9. Haglind, F. Design of aero gas turbines using hydrogen. *ASME* **2006**, *128*, 754–764. [CrossRef]
10. Apostolidis, A.; Sampath, S.; Laskaridis, P. WebEngine: A Web-Based Gas Turbine Performance Simulation Tool. In Proceedings of the ASME Turbo Expo 2013: Turbine Technical Conference and Exposition, San Antonio, TX, USA, 3–7 June 2013.
11. Villarreal, D.C. Digital Fuel Control for a Lean Premixed Hydrogen-Fueled Gas Turbine Engine. Master's Thesis, Virginia Tech, Blacksburg, VA, USA, 2009.
12. Arsalis, A. Thermodynamic modeling and parametric study of a small-scale natural gas/hydrogen-fueled gas turbine system for decentralized applications. *Sustain. Energy Technol. Assess.* **2019**, *36*, 100560. [CrossRef]
13. Osigwe, E.O. Thermodynamic Performance and Creep Life Assessment Comparing Hydrogen- and Jet-Fueled Turbofan Aero Engine. *Appl. Sci.* **2021**, *11*, 3873. [CrossRef]
14. Abedi, H. Preliminary Analysis of Compression System Integrated Heat Management Concepts Using LH2-Based Parametric Gas Turbine Model. *Aerospace* **2022**, *14*, 216. [CrossRef]
15. Verbeke , J.T. The Newton-Raphson method. *Int. J. Math. Educ. Sci. Technol.* **1995**, *26*, 177–193. [CrossRef]
16. Huang, K.M. Real time aeroengine model based on non iterative method. *Aerosp. Eng.* **2004**, *30*, 35–38. (In Chinese)
17. Sugiyama, N.T. Derivation of system matrices from nonlinear dynamic simulation of jet engines. *J. Guid. Control. Dyn.* **1994**, *17*, 1320–1326. [CrossRef]
18. Kong, X.; Wang, X.; Tan, D. A non-iterative aeroengine model based on volume effect. In Proceedings of the AIAA Modeling and Simulation Technologies Conference, Montreal, QC, Canada, 6–9 August 2001; p. 6623.
19. Anderson, J. *Fundamentals of Aerodynamics (SI Units)*; McGraw Hill: New York, NY, USA, 2011.
20. Chen, D.Z. Analysis and Research on Gas Turbine Cycle Scheme with Water Spray in Combustion Chamber. *J. Xi'An Jiaotong Univ.* **1962**, *1*, 64–75. (In Chinese)
21. Jing, G. Research on Water Injection Test for Emissions Reduction of Dual Fuel Combustor of Aero Derivative Gas Turbine. *Gas Turbine Technol.* **2016**, *29*, 49–52. (In Chinese)
22. Lin, J.Y. Research on NOx emission control and water spray technology of internal combustion engine exhaust. *Straits Sci.* **2016**, *12*, 81–83. (In Chinese)
23. Yuan, L.Y. Application of water spray technology in engine. *Intern. Combust. Engine Parts* **2016**, *12*, 81–83. (In Chinese)
24. Fong Q; Li SW. *Engineering Thermodynamics*; Northwestern Polytechnical University Press: Xi'an, China, 2006.
25. Li, W. Technology and Development Trend of Hydrogen Gas Turbine. *Hydrog. Powered Aviat.* **2022**, *2*, 39–42. (In Chinese)
26. Bahr, D. Aircraft Turbine Engine NOx Emission Abatement. In *Unsteady Combustion*; Springer: Berlin/Heidelberg, Germany, 1996.
27. Cao, M.D. Research on Optimization Design and Emission Analysis Methods of Civil Aircraft Engines. Ph.D. Thesis, Northwest University of Technology, Xi'an, China, 2016.
28. Simulink-Wikipedia. Available online: https://en.wikipedia.org/wiki/Simulink (accessed on 30 December 2022).

29. Wet Low NOx-Enwa. Available online: https://www.enwa.com/water-technology/market-segments/maritime-offshore-oil-gas/offshore-oil-gas-applications/injection-water/wet-low-nox (accessed on 30 December 2022).
30. Ohkubo, T. Low-NOx combustion technology. *Target* **2005**, *30*, 24.
31. Hung, W.S.Y. ; Agan, D.D. The Control of NOx and CO Emissions From 7-MW Gas Turbines with Water Injection as Influenced by Ambient Conditions. In Proceedings of the Turbo Expo: Power for Land, Sea, and Air, American, Houston, TX, USA, 18–21 March 1985; p. 79399.
32. Speedgoat. Real-Time Simulation and Testing. Available online: https://www.speedgoat.com/ (accessed on 30 December 2022).